Strojniški vestnik - Journal of Mechanical Engineering 59(2013)11, 689-696
DOI:10.5545/sv-jme.2013.999
Special Issue, *Original Scientific Paper*
Received for review: 2013-01-22
Received revised form: 2013-03-07
Accepted for publication: 2013-03-13

An Initial Study of Aerosol Jet® Printed Interconnections on Extrusion-Based 3D-Printed Substrates

Frederik Vogeler* – Wesley Verheecke – André Voet – Hans Valkenaers
[1] Thomas More University College Mechelen, Belgium

The combination of different additive manufacturing techniques to produce freeform products with multifunctional properties is gaining increasing popularity. In the research presented, Aerosol Jet® Printing (AJP) is combined with extrusion-based 3D printing. AJP starts with an ink to create micro-tracks. These tracks commonly have widths ranging from a few micrometers up to several millimeters and track heights ranging from a few tenths of a micrometer up to several micrometers, unlike extrusion-based 3D printers with which the extruded material usually has a resolution of tenths of millimeters. AJP can therefore be a complementary technique for extrusion-based 3D printing; in this manner, fine high resolution features can be added onto relatively rapidly produced extrusion-based 3D printed parts. Furthermore, AJP can be used to produce electrically conductive tracks to create interconnections, inductors, capacitors, strain gauges, etc.

In this paper, the creation of AJP-manufactured interconnects on extrusion-based 3D printed substrates is investigated. The relevant AJP process parameters to take into account are the flow rates of the aerosol, the flow rate of the sheath gas, the temperature settings of the ink and substrate, and the platform speed and nozzle-to-substrate distance. To obtain reliable results, the AJP process parameters are optimized for printing single-layered and multilayered silver ink tracks on extrusion-based 3D-printed surfaces. Important quality output parameters include the dimensions and the electrical properties of the printed interconnects.

Keywords: aerosol jet® printing, extrusion-based 3D printing, silver ink, interconnects, printed tracks, conductive tracks

0 INTRODUCTION

0.1 Key Benefits of Hybrid Additive Manufacturing

Additive Manufacturing (AM) [1] is no longer merely used as a production method for creating prototypes; today, it is more often used to create products with a high added value. Although there is still room for the optimization of individual AM processes, it is most likely that the next trend in AM is the combination of AM techniques, which can have a number of advantages, e.g. improving the accuracy of an AM process or creating multi-material products.

In the presented research, extrusion-based 3D printing is combined with Aerosol Jet® Printing (AJP). Extrusion-based 3D printing is typically used to create functional plastic (commonly ABS, PC or PLA) parts with sizes ranging from a cubic centimetre up to a cubic metre. AJP, in contrast, is used to create parts with micro-sized features. It is also frequently used to create printed electronics, including interconnects, resistors, inductors, capacitors, etc. In our research, AJP is used to print conductive tracks on extrusion-based 3D-printed parts.

A fundamental reason combining these technologies has so much potential is because of the feasibility of combining both techniques on the same machine. Both techniques are categorized as direct write technologies [2], they only require an *xyz* manipulation stage and a material deposition head.

0.2 Extrusion-Based 3D Printing

Extrusion-based 3D printing [3] is a generic term for all AM processes that utilize a head that deposits material by extruding viscous materials through a nozzle. The most commonly known extrusion-based 3D-printing technique is Fused Deposition Modeling™ (FDM®) [4] and [5]. This technique heats up a filament before pushing it through a fine opening.

Extrusion-based 3D printing usually has a resolution ranging from hundred to several hundred micrometres.

0.3 Aerosol Jet® Printing

AJP uses an ink as a starter material to build up products [6] to [9]. The ink is transformed into an aerosol by the atomizer. There are several ways of atomizing liquids, depending on the type of atomizer used [10] and [11]. In this research, a pneumatic atomizer is used. It creates a nebula of the ink by sending carrier gas through a venturi. The venturi creates a vacuum that sucks the ink through a narrow tube of a few millimetres in diameter. The ink is then sent through an opening and turned into droplets. The amount of carrier gas that is fed to the atomizer is called the 'atomization gas flow'.

In the final stage, the aerosol is focused onto the substrate by adding a concentric flow of gas, which is called 'sheath gas'. Adding the sheath gas to the aerosol occurs inside the print nozzle, by sending

*Corr. Author's Address: Thomas More University, College Mechelen, J. De Nayerlaan 5, 2860 Sint-Katelijne-Waver, Belgium, frederik.vogeler@lessius.kuleuven.be

the gas along a conical shaft [12] to [16]. In the center of the conical shaft, the aerosol is added. An overview of the AJP process is given in Fig. 1.

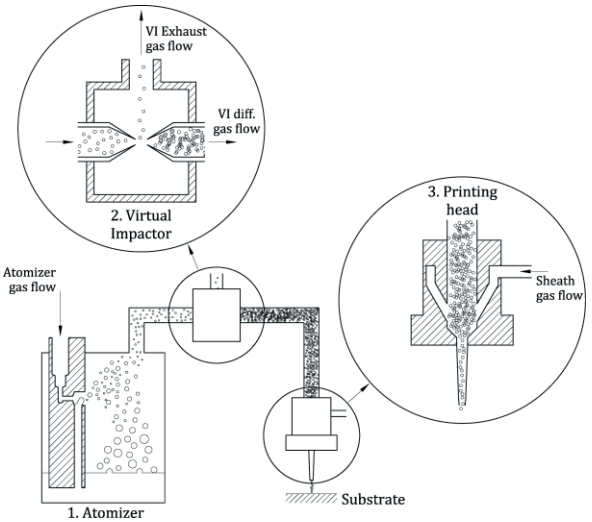

Fig. 1. *Overview of the AJP process*

Because the flow coming directly out of the pneumatic atomizer is too high for the nozzle to handle, an extra element is placed between the atomizer and nozzle. This element is called the 'Virtual Impactor' (VI). It reduces the aerosol flow by taking away some of the carrier gas (and small aerosol droplets) [17] to [23]. Inside the VI, the aerosol tube is interrupted, and gas is sucked out of the VI. Due to the mass inertia of the droplets, the larger aerosol droplets continue a straight trajectory and are not sucked out of the VI; smaller droplets and carrier gas are sucked out. The flow that is taken away from the aerosol is called the 'VI exhaust'. The difference between the atomizer flow and VI exhaust flow is fed to the nozzle; this is referred to as the 'VI difference'.

Depending on the processed material, substrate material and conditions, process settings and nozzle-size single-printed track widths can vary from just a few micrometres up to several millimetres [24] to [26]. Track heights can range from a few tenths of a micrometre up to several micrometres.

1 SETUP OF THE EXPERIMENT

The substrate samples in the following experiments are produced on a Stratasys Dimension® SST1200es machine, from ABSplus™-P430 plastic. The test samples have a rectangular shape with a height of 8 mm. An isometric sketch of the substrate samples is shown in Fig. 2.

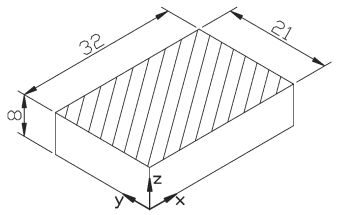

Fig. 2. *Isometric view of the substrate; all dimensions are displayed in millimetres*

The samples were built up layer by layer in the z direction indicated by Fig. 2; they were filled with cross hatching. On the top surface, indicated by hatching in Fig. 2, test circuitry is printed by means of AJP. The top surface was first sanded down for half a minute, with silicon carbide P220 sand paper on a horizontal disk sander. Untreated samples from the used 3D printer have a surface roughness that is too high for the robust printing of silver ink tracks. This problem can be resolved by printing on parts with a finer cross hatching or using an ink-substrate combination with better wetting properties. In all the used samples, the sanding resulted in an average *Ra* value of 1.42 µm, with a standard deviation of 0.73 µm. This is a relatively large surface roughness compared to other substrates for printed electronics (e.g. glass or polyimide foil). The influence of the level of abrasion on the AJP result has not been investigated and will be included in future research. Before the samples were placed inside the AJP machine, the surface was treated with isopropanol to cleanse the surface and reinsure a repeatable substrate surface. The samples were first sanded down because preliminary tests showed that untreated samples gave insufficient adhesion between the printed ink and substrate.

To investigate the conductivity of AJP tracks, circuitry was designed, shown in Fig. 3. Four square probing patches were to perform a 4-point probing test over a track length of 10 mm.

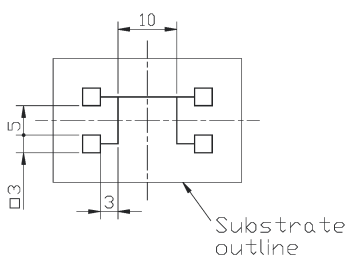

Fig. 3. *Dimensions of the test circuitry; all dimensions are displayed in millimetres*

The circuitry was printed with Cabot CSD-32® material, a commercially available ink based on silver

nanoparticles (45 to 55 wt%), used as conductive filler material in ethylene glycol. The silver particles have a size of less than 60 nm and are wrapped in a polymer coating. To reinsure conductivity, the material supplier suggests sintering the printed material. Greer et al. 2007 [27] showed that sintering temperatures of nanoparticle silver inks should at least reach 150 °C in order to reach adequate conductive behavior. Because the glass transition temperature of ABS is about 100 °C, printed samples were cured in an oven at 80 °C for only 1.5 hours.

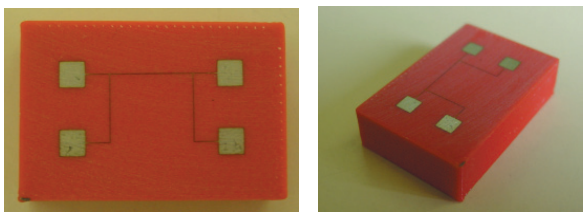

Fig. 4. *Photographs of a finished sample*

During the experiments, the hardware setup of the AJP machine was unchanged. A nozzle with an opening of 300 µm was used to produce all the samples. Although smaller nozzle sizes are available and would provide smaller print resolution, such nozzles are probably not appropriate for this initial study. By having a smaller print resolution, tracks will have smaller cross sections, making it more difficult to obtain conductive behavior.

2 ANALYSIS OF THE PRINTED CIRCUITRY

To analyze the electrical conductivity of the produced samples (Fig. 4), a Keithley® 580 micro-ohmmeter was used. The maximum resistivity that could be measured is 200 kΩ. Samples that have a higher resistivity are considered to have no conductive properties.

The dimensions of the tracks were quantified with both a Digi-Microscope 500X Series vision system and a Taylor-Hobson® tactile 2D profile measuring device.

The vision system consists of a USB-microscope placed perpendicular to the substrate. Unfortunately, this method cannot give information about the height (z direction) of a printed track. Important information that it does provide is the track width and that smoothness of the track edges. To determine these parameters, the edges of the track were first determined with the algorithm described by [28], a few examples of the result of this edge detection algorithm are given in Fig. 5. For the edge smoothness, the arithmetic average of the detected edges was calculated. In Eq. (1), the average edge smoothness is represented by ES_a in µm, n represents the number of detected points on an edge and x_i is the shortest distance in µm from a detected point to the line fitted through all detected points. The edge smoothness will become salient when several tracks need to be printed side by side.

$$ES_a = \frac{1}{n}\sum_{i=1}^{n}\left|x_i\right|. \tag{1}$$

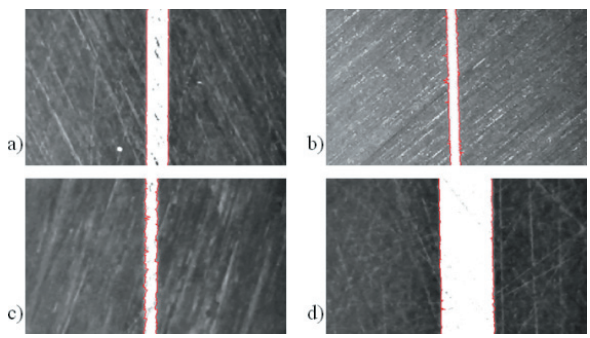

Fig. 5. *Examples of the edge detection algorithm from the vision system for various types of printed AJP tracks*

A 2D profile system was used to create an intersection profile of the track. This system gives information about the track width, height and cross section area. The downside of this system is that when printing only one layer of material it is impossible to differentiate the printed track from the substrate roughness profile. Consequently, this system was only used for analyzing the circuitries produced with multiple layers. Fig. 6 shows an example of an intersection measured with the 2D profile system.

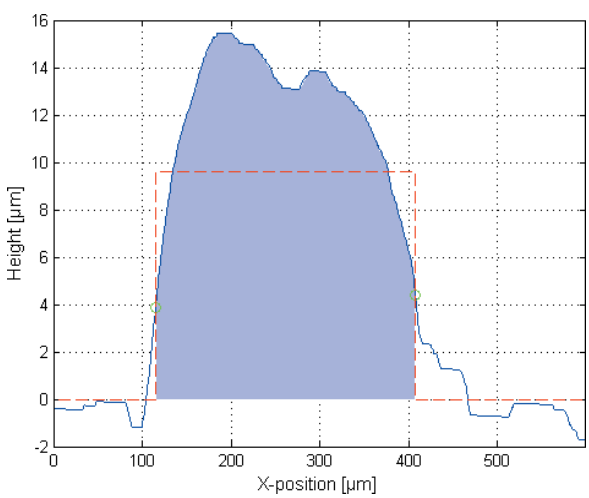

Fig. 6. *Examples of a measured intersection of a track, produced by printing 5 tracks side by side and 5 layers*

3 INVESTIGATION OF THE PROCESS PARAMETERS

3.1 VI Difference and Temperature Settings

In a first set of tests, the VI difference and temperature settings of the AJP process were investigated. For this test, the previously presented circuitry was printed with one track and one layer. Regarding the AJP process, only the VI exhaust gas, printing head temperature and substrate temperature were changed. The atomizer gas flow was set to 133.33 × 10^{-7} m^3/s (800 cm^3/min) and the sheath gas flow was set to 10.83 × 10^{-7} m^3/s (65 cm^3/min); the printing speed was set to 8 mm/s and the nozzle-to-substrate distance was set to 3 mm.

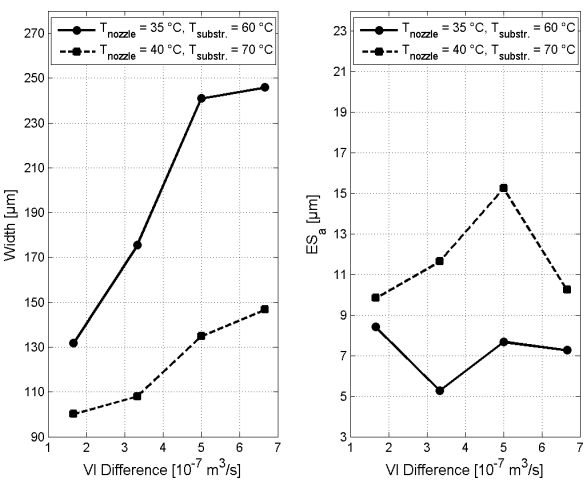

Fig. 7. *The VI difference and temperature settings*

Fig. 7 shows the results of the VI difference and temperature settings tests. As expected, the width of the track rises as the VI difference increases, causing the nozzle to deposit more aerosol per time unit. The high possibility of a (statistical) relationship between track width and VI difference is also confirmed by the correlation coefficients. For printing at low temperatures, an *r*-value (correlation coefficient) of 0.96 was obtained and at high temperatures an *r*-value of 0.98. In practice, attempting to control the track width using the VI difference is recommended.

Concerning the edge smoothness, correlation with the VI difference is exceptionally low: for the test at low temperatures, an *r* value of –0.10 was obtained; for the test at high temperatures, an *r* value of 0.25 was obtained.

Processing temperatures do seem to have an influence on both the track width and the edge smoothness. Printing at higher temperatures generates narrower tracks but generates a larger edge smoothness. A higher temperature of the nozzle will evaporate more solvent in the aerosol droplets before they reach the substrate, changing the concentration of silver particles in the aerosol droplets. This higher concentration of silver particles causes the ink to act in a more viscous manner; once deposited, less ink will flow on the substrate. A higher temperature of the substrate will increase the effect of the reduced flow of the ink droplets on the substrate. The resistivity of the samples was too high to measure.

3.2 Sheath Gas Setting

The second set of tests concerned the sheath gas settings. In this series of tests, the sheath gas was altered. Furthermore, two sets of VI difference where tested: one at 4.17 × 10^{-7} m^3/s (25 cm^3/min) and one at 2.50 × 10^{-7} m^3/s (15 cm^3/min). The atomizer gas flow and printing speed was set the same as in the tests described in Section 3.1. The temperature of the nozzle was set at 35 °C and the substrate temperature at 60 °C. Only one track was printed in one layer.

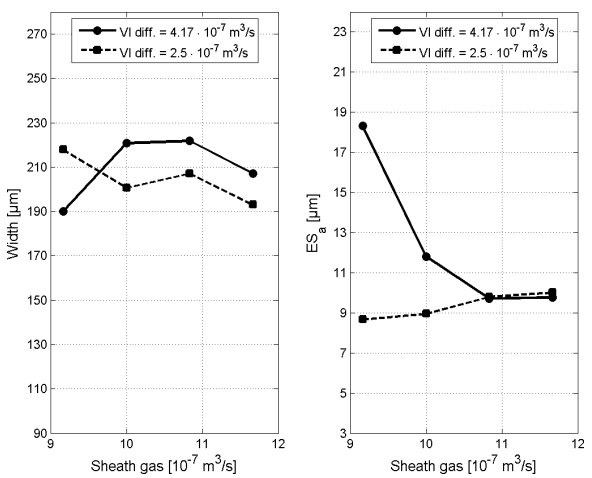

Fig. 8. *The sheath gas setting*

Fig. 8 shows the results of the sheath gas and VI difference tests. As demonstrated by the previous test, the tracks become wider when the VI difference becomes larger; only the first point in the left graph of Fig. 8 shows a smaller track for a larger VI difference. It is most likely that the first value of the VI difference of 4.17 × 10^{-7} m^3/s (25 cm^3/min) is an outlier.

The correlation coefficient between the width and sheath gas setting is 0.45 for the higher VI difference setting and –0.84 for the lower VI difference setting. These values indicate that using the sheath gas to control the track width is not the best option. According to the results of Section 3.1, it would be

better to use the VI-difference for controlling the track width.

The edge smoothness, however, seems to correlate better with the sheath gas settings. For a VI difference of 4.17 × 10^{-7} m^3/s (25 cm^3/min), the correlation is –0.88, for a VI difference of 2.50 × 10^{-7} m^3/s (15 cm^3/min), the correlation is 0.97. The fact that correlation is negative for a higher setting of VI difference compared to the lower settings of VI difference indicates that the edge smoothness is influenced by the combination of VI difference and sheath gas. In practice, sheath gas is a good candidate for controlling the edge smoothness.

The resistivity of the samples was, as in the tests of Section 3.1, too high to measure.

3.3 Nozzle-to-Substrate Distance

In the next test, the nozzle-to-substrate distance was investigated. The aerosol can only be focused within certain boundaries of the nozzle-to-substrate distance.

For this test, the atomizer gas flow and printing speed was set the same as in Sections 3.1 and 3.2; sheath gas was set at 9.17 × 10^{-7} m^3/s (55 cm^3/min), VI difference at 3.33 × 10^{-7} m^3/s (20 cm^3/min), the temperature of the nozzle was set at 50 °C and the temperature of the substrate was set at 75 °C. As in the previous tests, the samples consisted of one printed track in one layer.

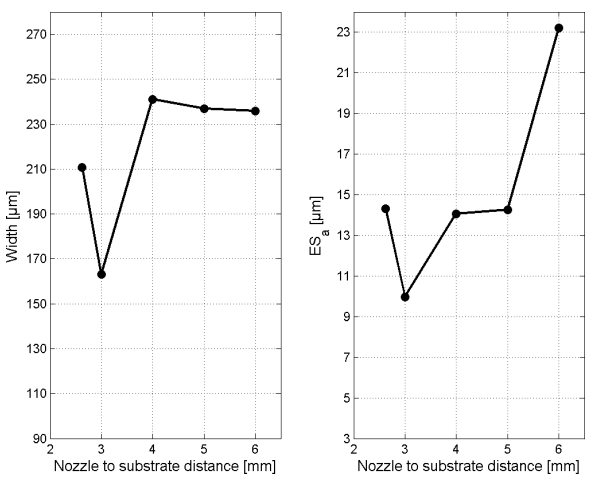

Fig. 9. *The nozzle to substrate distance*

This test shows the importance of the nozzle-to-substrate distance. Fig. 9 shows that the ideal focusing position is around 3 mm; not only is the track width that smallest, but also the edge smoothness is smallest for this position. Furthermore, the track width seems to stagnate for a nozzle-to-substrate distance larger than 4 mm, while the edge smoothness seems to become bigger with a larger nozzle-to-substrate distance.

As with the samples in Sections 3.1 and 3.2, none showed signs of conductivity. Consequently, several tracks side by side or several layers of material are needed in order to create functional interconnections. In the next set of tests, several tracks are printed side by side and several layers of material are deposited.

3.4 Multiple Tracks Side by Side

During this test, the circuitry is printed with several tracks side by side. To reinsure overlap between the tracks, the parallel central axes of the tracks are printed 50 µm apart. Atomizer gas flow and printing speed were set as before (Sections 3.1 to 3.3), nozzle temperature was set to 50 °C, substrate temperature to 80 °C, sheath gas was set at 10.83 × 10^{-7} m^3/s (65 cm^3/min) and VI difference was set at 5.00 × 10^{-7} m^3/s (30 cm^3/min).

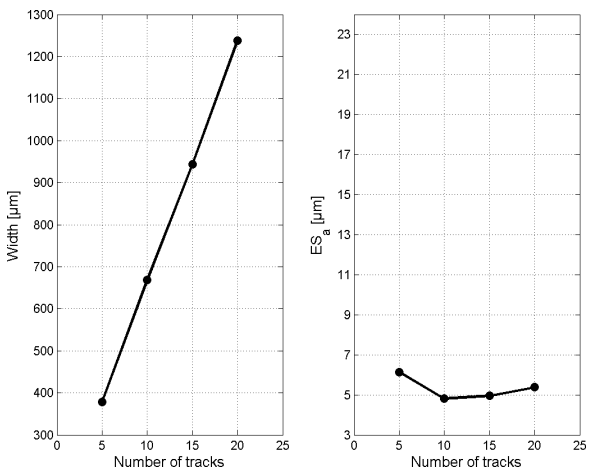

Fig. 10. *Number of tracks side by side*

Fig. 10 shows an obvious linear behavior for the width in function of the number of tracks side by side (*r* value of 1.00). The edge smoothness does not show a trend (*r* value of –0.46). The edge smoothness for multiple tracks side by side is significantly lower than the edge smoothness for samples consisting of only a single track.

The first sample of only five tracks side by side gave no conductivity. The last sample of 20 tracks side by side gave a resistivity of 67.4 kΩ; this is probably an outlier. The remaining two samples gave a resistance of 99.61 Ω (10 tracks side by side) and 11.24 Ω (15 tracks side by side).

3.5 Multiple Layers

In the final test, the number of layers in the functions of the width, edge smoothness, resistivity, track height and cross section of the track were examined. The same AJP settings were used as in Section 3.4. The circuitry was printed with five tracks side by side, with the parallel central axes of the tracks printed 50 µm apart. Only two samples were created: one with three layers and one with five layers.

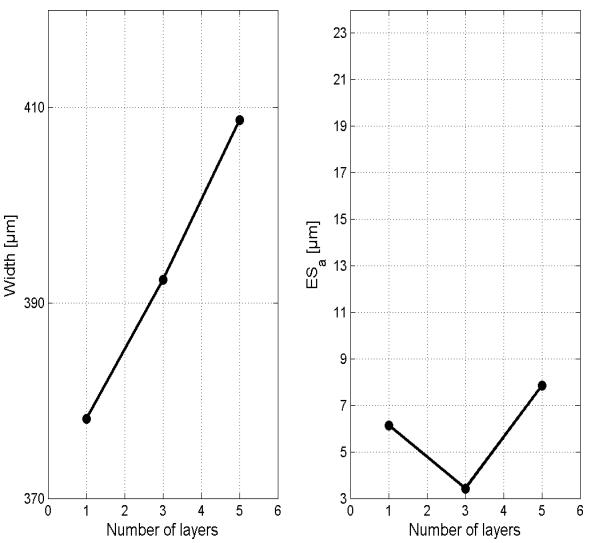

Fig. 11. *The number of layers*

Fig. 11 shows that the width of the track increases with the number of printed layers. This suggests that not all material printed onto an existing layer remains upon that layer, but tends to run down the side of the layer. For printing mere interconnections, this is not a problem; this might, however, cause a problem when trying to use AJP as a 3D printing technique. Just as in the early days of direct 3D inkjet printing, getting droplets to remain upon a new layer proved to be one of the most challenging tasks. As with multiple tracks printed side by side, no trend was observed (r-value of 0.38) for the edge smoothness.

As mentioned in Section 3.4, one layer of five tracks side by side gave no conductivity. Three and five layers gave conductivity of 24.75 and 20.61 Ω, respectively. However, one layer of 15 tracks printed side by side (Section 3.4) gave a lower resistance than five layers of five tracks printed side by side. Therefore, considering processing time, it would be more beneficial to print several tracks side by side in order to obtain better electrical properties. However, printing several tracks side by side does result in broader tracks.

In practice, choosing the number of tracks side by side and number of layers will be a consideration based on electrical properties, track width and processing time. A simple alternative for obtaining conductivity is merely using a nozzle with a bigger opening. This will allow the creation of wider tracks and will require less processing time.

Multiple layers can be distinguished from the roughness profile of the substrate. Therefore, it was possible to measure the track profile. The track profile was measured at three locations. From each measurement, the track height and cross section area was extracted. The results of these measurements are displayed in Fig. 12. The figure shows the average value and, minimum and maximum measured value (indicated by the error bars). The graphs show no surprises, both the track height as well as the cross section increase with the number of layers.

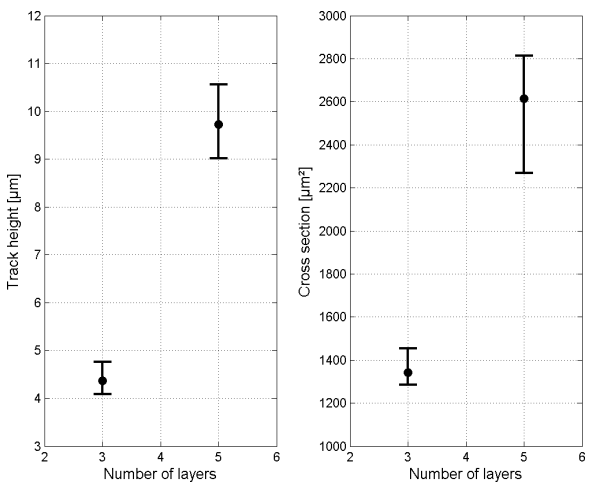

Fig. 12. *The number of layers*

What might seem strange is that there is no one-to-one relationship between the number of layers and the track height; furthermore, the left graph of Fig. 12 seems to indicate a growing increase in height in relation to the number of layers (3 layers give a height of 4.4 µm; 5 layers give a height of 9.7 µm). There are a number of probable causes for this phenomenon, which need to be investigated in the future. First, the wetting behavior of the first layer is different than that of the following layers as the first layer is deposited onto the ABS substrate, in contrast to the other layers that are deposited onto printed material. Other possible causes could be the slumping or mixing of not fully dried layers, causing an increase of the width of the previous printed track.

4 CONCLUSION AND DISCUSSION

In this paper, circuitry for testing the conductivity was printed with silver ink, by means of AJP, onto a substrate manufactured with extrusion-based 3D printing. Although the substrate was first sanded down in order to generate the proper surface characteristics, this preliminary research mentions some key aspects towards combining extrusion-based 3D printing and AJP. The main focus of the research was understanding the relationship between the AJP process settings and the dimensional and electrical properties of the printed interconnects. To date, only a limited set of experiments have been performed; future research will also have to include the repeatability of the process, as the presented tests are limited. Other aspects to obtain better and repeatable printing and conductive behavior will also have to be examined, e.g. other hardware setups, proper sintering methods, other conductive inks, surface activation, etc. Nevertheless, this work will be a good starting point for future research in this area.

Based on correlation studies, when printing single tracks, the VI-difference is probably the best choice for controlling track width; the edge smoothness is best controlled by the sheath gas settings. Printing single tracks, however, gave no electrical conductive properties to the tracks. As a result, multiple tracks or layers of material are required in order to generate sufficient conductive properties. The presented research shows that, considering processing time, printing several tracks side by side is more beneficial than printing multiple layers. Although in practice making a choice in number of tracks side by side and layers will also consider the required resolution of the interconnects.

5 ACKNOWLEDGEMENTS

The authors would like to thank the IWT for their support in the PO7810-EUR-ERA-01 project within the framework of the TETRA/ EraSME 3DAMEEA.

6 REFERENCES

[1] Kruth, J.-P., Leu, M.C., Nakagawa, T. (1998). Progress in additive manufacturing and rapid prototyping. *CIRP Annals - Manufacturing Technology*, vol. 47, no. 2, p. 525-540, DOI:10.1016/S0007-8506(07)63240-5.

[2] Hon, K.K.B., Li, L., Hutchings, I.M. (2008). Direct writing technology - Advances and developments. *CIRP Annals - Manufacturing Technology*, vol. 57, no. 2, p. 601-620, DOI:10.1016/j.cirp.2008.09.006.

[3] Singamneni, S., Roychoudhury, A., Diegel, O., Huang, B. (2012). Modeling and evaluation of curved layer fused deposition. *Journal of Materials Processing Technology*, vol. 212, no. 1, p. 27-35, DOI:10.1016/j.jmatprotec.2011.08.001.

[4] Ahn, D., Kweon, J.-H., Kwon, S., Song, J., Lee, S. (2009). Representation of surface roughness in fused deposition modeling. *Journal of Materials Processing Technology*, vol. 209, no. 15-16, p. 5593-5600, DOI:10.1016/j.jmatprotec.2009.05.016.

[5] Anitha, R., Arunachalam, S., Radhakrishnan, P. (2001). Critical parameters influencing the quality of prototypes in fused deposition modeling. *Journal of Materials Processing Technology*, vol. 118, no. 1-3, p. 385-388, DOI:10.1016/S0924-0136(01)00980-3.

[6] US Patent No. 7,938,341 B2 (2011). *Miniature Aerosol Jet and Aerosol Jet Array*. United States Patent and Trademark Office, Alexandria.

[7] Marple, V.A., Olson, B.A. (2011). *Aerosol Science and Technology: History and Reviews*, RTI Press, Research Triangle park, p. 509-528, DOI:10.3768/rtipress.2011.bk.0003.1109.

[8] US Patent No. 7,108,894 B2 (2006). *Direct WriteTM System*. United States Patent and Trademark Office, Alexandria.

[9] US Patent No. 2003/0228124 A1 (2003). *Apparatus and Method for Maskless Mesoscale Material Deposition*, United States Patent and Trademark Office, Alexandria.

[10] Bailey, A.G. (1974). The generation and measurement of aero-sols. *Journal of Materials Science*, vol. 9, no. 8, p. 1344-1362, DOI:10.1007/BF00551854.

[11] Fängmark, I., Carpin, J.C. (1998). Stability of unrease during aerosolization: the effect of operating conditions. *Journal of Aero-sol Science*, vol. 29, no. 3, p. 279-288, DOI:10.1016/S0021-8502(97)10010-6.

[12] Akhatov, I.S., Hoey, J.M., Swenson, O.F., Schulz, D.L. (2008). Aerosol focusing in micro-capillaries: Theory and experiment. *Journal of Aerosol Science*, vol. 39, no. 8, p. 691-709, DOI:10.1016/j.jaerosci.2008.04.004.

[13] Fernández De La Mora, J., Riesco-Chueca, P. (1988). Aerodynamic focusing of particles in a carrier gas. *Journal of Fluid Mechanics*, vol. 195, p. 1-21, DOI:10.1017/S0022112088002307.

[14] Lee, K.-S., Kim, S., Lee, D. (2009). Aerodynamic focusing of 5–50nm nanoparticles in air. *Journal of Aerosol Science*, vol. 40, no. 12, p. 1010-1018, DOI:10.1016/j.jaerosci.2009.09.004.

[15] US Patent No. 2009/0309014 A1 (2009). *Method and Apparatus to Sharply Focus Aerosol Particles at High Flow Rate and a Wide Range of Sizes*. United States Patent and Trademark Office, Alexandria.

[16] Wang, X., Kruis, F.E., McMurry, P.H. (2005). Aerodynamic Focusing of Nanoparticles: I. Guidelines for Designing Aerodynamic Lenses for Nanoparticles. *Aerosol Science and Technology*, vol. 39, no. 7, p. 611-623, DOI:10.1080/02786820500181901.

[17] Ding. Y., Koutrakis. P. (2000). Development of a dichotomous slit nozzle virtual impactor. *Journal*

of Aerosol Science, vol. 31, no. 12, p. 1421-1431, DOI:10.1016/S0021-8502(00)00048-3.

[18] Haglund, J.S., McFarland, A.R. (2004). A circumferential slot virtual impactor. *Journal of Aerosol Science and Technology*, vol. 38, p. 664-674, DOI:10.1080/02786820490486015.

[19] Lee, P., Chen, D.-R., Pui, D.Y.H. (2003). Experimental study of a nanoparticle virtual impactor. *Journal of Nanoparticle Research*, vol. 5, no. 3-4, p. 269-280, DOI:10.1023/A:1025538930994.

[20] Lim, K.S., Lee, K.W. (2006). Collection efficiency and particle loss of virtual impactors with different methods of increasing pressure drop. *Journal of Aerosol Science*, vol. 37, no. 10, p. 1188-1197, DOI:10.1016/j.jaerosci.2005.11.011.

[21] Loo, B.W., Cork, C.P. (1988). Development of High Efficiency Virtual Impactors. *Journal of Aerosol Science and Technology*, vol. 9, no. 3, p. 167-176, DOI:10.1080/02786828808959205.

[22] Noone, K.B., Heintzenberg, J. (1991). On the determination of droplet size distributions with the counterflow virtual impactor. *Journal of Atmospheric Research*, vol. 26, no. 5, p. 389-405, DOI:10.1016/0169-8095(91)90060-A.

[23] US Patent No. 4,767,524 (1988). *Virtual Impactor.* United States Patent and Trademark Office, Alexandria.

[24] Matsusaka, S., Theerachaisupakij, W., Yoshida, H., Masuda, H. (2001). Deposition layers formed by a turbulent aerosol flow of micron and sub-micron particles. *Journal of Powder Technology*, vol. 118, no. 1-2, p. 130-135, DOI:10.1016/S0032-5910(01)00303-5.

[25] Pál, E., Zöllmer, V., Lehmhus, D., Busse, M. (2011). Synthesis of Cu0.55Ni0.44Mn0.01 alloy nanoparticles by solution combustion method and their application in aerosol printing. *Journal of Colloids and Surfaces*, vol. 384, no. 1-3, p. 661-667, DOI:10.1016/j.colsurfa.2011.05.038.

[26] Parker, S., Foat, T., Preston, S. (2008). Towards quantitative prediction of aerosol deposition from turbulent flows. *Journal of Aerosol Science*, vol. 39, no. 2, p. 99-112, DOI:10.1016/j.jaerosci.2007.10.002.

[27] Greer, J.R., Street, R.A. 2007. Thermal cure effects on electrical performance of nanoparticle silver inks. *Journal of Acta Materialia*, vol. 55, no. 18, p. 6345-6349, DOI:10.1016/j.actamat.2007.07.040.

[28] Vogeler, F., Verheecke, W., Voet, A. (2012). Vision system based 2D quality control of micro aerosol jet printed tracks. *Optical Measurement Techniques for Systems & Structures², Proceedings of the 12th International OPTIMESS Conference 2012*, p. 445-457.